

A NEW DYNAMIC GGDH SUBGRID-SCALE HEAT FLUX MODEL FOR LARGE-EDDY SIMULATION OF TURBULENT THERMAL FLOWS

Bing-Chen Wang, Eugene Yee

Defence Research & Development Canada — Suffield
P.O. Box 4000, Medicine Hat, Alberta, T1A 8K6, Canada
E-mail: bingchen.wang@drdc-rddc.gc.ca, eugene.yee@drdc-rddc.gc.ca

Donald J. Bergstrom, Jing Yin

Dept. of Mechanical Engineering, Univ. of Saskatchewan
Saskatoon, Saskatchewan, S7N 5A9, Canada
E-mail: don.bergstrom@usask.ca, jiy080@mail.usask.ca

ABSTRACT

In this research, two new dynamic tensor diffusivity subgrid-scale (SGS) heat flux (HF) models are proposed for large-eddy simulation (LES) of thermal convection. The linear and nonlinear constitutive relations for these two new modelling approaches represent the most general explicit algebraic formulations possible for the family of SGS HF models constructed using the resolved temperature gradient and SGS stress tensor. As a result, these two proposed models include a number of previous dynamic SGS HF models as special cases. In contrast to the conventional dynamic eddy thermal diffusivity SGS HF model, both proposed models admit more degrees of freedom, allow non-alignment between the SGS heat flux and negative resolved temperature gradient vectors, and therefore, provide a more realistic geometrical and physical representation for the SGS heat flux vector. To validate the proposed models, numerical simulations have been performed based on a benchmark test case of an unstably stratified horizontal channel flow.

INTRODUCTION

The application of a dynamic procedure to SGS HF modelling was introduced by Moin *et al.* (1991), shortly after the proposal of the dynamic SGS stress model by Germano *et al.* (1991). In their work, Moin *et al.* (1991) proposed a *dynamic eddy diffusivity model for representing the SGS heat flux* (DEDM-HF). DEDM-HF is based on a linear constitutive relation analogous to Fourier's law for describing molecular heat conduction, which assumes that the SGS HF vector is instantaneously proportional to and aligned with the negative resolved temperature gradient, viz. $h_j \propto -\partial\bar{\theta}/\partial x_j$. It is known (Salveti and Banerjee, 1995; Peng and Davidson, 2002; Porté-Agel *et al.*, 2001) that such an overly simplified linear constitutive relation is inconsistent with the physics of turbulent convection and cannot correctly reflect the local geometrical property of the SGS HF vector.

During the past decade, dynamic SGS HF models progressed from models of the eddy diffusivity type to those based on a tensor diffusivity in order to further improve the physical and geometrical representation of the SGS HF vector. Salvetti and Banerjee (1995) introduced a *dynamic two-parameter mixed model for representing the SGS heat flux* (DTPMM-HF), which combines the linear eddy diffusivity SGS HF model with a scale-similarity SGS HF model. By using a truncated Taylor series expansion for analysis of a filtered flow variable, Porté-Agel *et al.* (2001) and Kang and Meneveau (2002) introduced a simplified DTPMM-HF for studying heat fluxes and dissipation in an atmospheric boundary layer. Peng and Davidson (2002) proposed a *dynamic homogeneous linear tensor diffusiv-*

ity model (DHLTDM-HF) for studying a buoyancy driven turbulent flow. In the approach of Peng and Davidson, the tensor diffusivity is constructed as a homogeneous linear function of the resolved strain rate tensor [defined as $\bar{S}_{ij} \stackrel{\text{def}}{=} (\partial\bar{u}_i/\partial x_j + \partial\bar{u}_j/\partial x_i)/2$]. Using the theory of tensor functions, Wang *et al.* (2006a, 2007) recently proposed a *dynamic inhomogeneous linear tensor diffusivity model* (DILTDM-HF) and a *dynamic nonlinear tensor diffusivity model* (DNTDM-HF) for representation of the SGS heat flux. The tensor diffusivity for DILTDM-HF is constructed as an inhomogeneous linear function of \bar{S}_{ij} and the resolved rotation rate tensor $\bar{\Omega}_{ij}$ [defined as $\bar{\Omega}_{ij} \stackrel{\text{def}}{=} (\partial\bar{u}_i/\partial x_j - \partial\bar{u}_j/\partial x_i)/2$] (Wang *et al.*, 2007); whereas, the tensor diffusivity for DNTDM-HF is constructed as a quadratic nonlinear function of \bar{S}_{ij} (Wang *et al.*, 2006a).

The previous approaches for dynamic SGS HF modelling represented by DEDM-HF, DTPMM-HF, DHLTDM-HF, DILTDM-HF and DNTDM-HF rely on the resolved velocity gradient tensor (or, its derivatives \bar{S}_{ij} and $\bar{\Omega}_{ij}$) for constructing the modelling constitutive relation. In contrast to these previous investigations, the objective of the current research is to extend the concept of *generalized gradient diffusion hypothesis* (GGDH) of Daly and Harlow (1970) to develop two new dynamic tensor diffusivity SGS HF models based on the SGS stress tensor τ_{ij} . In the current proposal, because the tensor diffusivity is a tensor function of τ_{ij} , the model for the SGS HF vector has more degrees of freedom (dependent on the choice of the SGS stress model), with the result that the concomitant constitutive relationship achieves greater generality in comparison with the conventional approaches.

SGS STRESS AND HEAT FLUX MODELS

In LES of thermal convection, the governing equations include the filtered continuity, momentum and thermal energy equations, which take the following form for an incompressible flow:

$$\frac{\partial \bar{u}_i}{\partial x_i} = 0, \quad (1)$$

$$\frac{\partial \bar{u}_i}{\partial t} + \frac{\partial (\bar{u}_i \bar{u}_j)}{\partial x_j} = -\frac{1}{\rho} \frac{\partial \bar{p}}{\partial x_i} + \nu \frac{\partial^2 \bar{u}_i}{\partial x_j \partial x_j} - \frac{\partial \tau_{ij}}{\partial x_j} - \beta g_i (\bar{\theta} - \Theta_r), \quad (2)$$

$$\frac{\partial \bar{\theta}}{\partial t} + \frac{\partial (\bar{u}_j \bar{\theta})}{\partial x_j} = \alpha \frac{\partial^2 \bar{\theta}}{\partial x_j \partial x_j} - \frac{\partial h_j}{\partial x_j}, \quad (3)$$

where $\bar{\theta}$ is the filtered temperature, $[g_i] = [0, -g, 0]^T$ is the gravitational acceleration vector, β is the thermal expansion coefficient, α is the molecular thermal diffusivity, and Θ_r is a reference temperature, which for our test case of an unstably stratified channel flow, is taken as the bulk temperature, viz. $\Theta_r = \theta_B = \int_0^{2\delta} \langle \bar{\theta} \rangle dx_2 / 2\delta$. Here, δ is the half channel width, and $\langle \cdot \rangle$ corresponds to a quantity averaged both in

time and over the homogeneous x_1 - x_3 plane. The streamwise, wall-normal and spanwise coordinates for the Cartesian frame used in this research are denoted using x_1 , x_2 and x_3 , respectively. As a consequence of the filtering process, the so-called SGS stress tensor and SGS HF vector appear in the above system of governing equations, which are defined as $\tau_{ij} \stackrel{\text{def}}{=} \overline{u_i u_j} - \bar{u}_i \bar{u}_j$ and $h_j \stackrel{\text{def}}{=} \overline{u_j \theta} - \bar{u}_j \bar{\theta}$, respectively. In the following two Subsections, the conventional and proposed modelling formulations for τ_{ij} and h_j , required for closing the above system of governing equations, are described.

SGS Stress Models

Two dynamic SGS stress models are tested in this research: namely, the conventional dynamic Smagorinsky model (DM) of Lilly (1992) and dynamic nonlinear SGS stress model (DNM) of Wang and Bergstrom (2005).

SGS Stress Model 1 (DM):

The constitutive relation for DM is based on a linear tensor function of the resolved strain rate tensor \bar{S}_{ij} , i.e.

$$\tau_{ij}^* = \tau_{ij} - \frac{\tau_{kk}}{3} \delta_{ij} = -2C_S \bar{\Delta}^2 |\bar{S}| \bar{S}_{ij}, \quad (4)$$

where $|\bar{S}| = (2\bar{S}_{ij}\bar{S}_{ji})^{1/2}$, $\bar{\Delta}$ is the grid-level filter width, and an asterisk represents a trace-free tensor, i.e., $(\cdot)_{ij}^* \stackrel{\text{def}}{=} (\cdot)_{ij} - (\cdot)_{kk} \delta_{ij}/3$. Following the dynamic procedure of Lilly (1992), the model coefficient C_S can be obtained as

$$C_S = -(M_{ij} \mathcal{L}_{ij}) / (M_{ij} M_{ij}), \quad (5)$$

where $\mathcal{L}_{ij} \stackrel{\text{def}}{=} \widetilde{\bar{u}_i \bar{u}_j} - \bar{u}_i \bar{u}_j$, and $M_{ij} \stackrel{\text{def}}{=} \alpha_{ij} - \tilde{\beta}_{ij}$ is a differential tensor with $\alpha_{ij} \stackrel{\text{def}}{=} 2\bar{\Delta}^2 |\bar{S}| \tilde{S}_{ij}$ and $\beta_{ij} \stackrel{\text{def}}{=} 2\bar{\Delta}^2 |\bar{S}| \bar{S}_{ij}$. In these equations, the filtered quantities at the grid-level are denoted using an overbar, while the filtered quantities at the test-grid-level are denoted using a tilde.

SGS Stress Model 2 (DNM):

The constitutive relation for the second tested SGS stress model DNM is based on an explicit nonlinear quadratic tensorial polynomial constitutive relation, viz.

$$\tau_{ij}^* = -C_S \beta_{ij} - C_W \gamma_{ij} - C_N \eta_{ij}, \quad (6)$$

where $\gamma_{ij} \stackrel{\text{def}}{=} 4\bar{\Delta}^2 (\bar{S}_{ik} \bar{\Omega}_{kj} + \bar{S}_{jk} \bar{\Omega}_{ki})$ and $\eta_{ij} \stackrel{\text{def}}{=} 4\bar{\Delta}^2 (\bar{S}_{ik} \bar{S}_{kj} - \bar{S}_{mn} \bar{S}_{nm} \delta_{ij}/3)$ are base tensor functions. It can be shown (Wang and Bergstrom, 2005) that the three model coefficients can be evaluated through optimization as

$$\begin{bmatrix} M_{ij} M_{ij} & M_{ij} W_{ij} & M_{ij} N_{ij} \\ W_{ij} M_{ij} & W_{ij} W_{ij} & W_{ij} N_{ij} \\ N_{ij} M_{ij} & N_{ij} W_{ij} & N_{ij} N_{ij} \end{bmatrix} \cdot \begin{bmatrix} C_S \\ C_W \\ C_N \end{bmatrix} = - \begin{bmatrix} \mathcal{L}_{ij}^* M_{ij} \\ \mathcal{L}_{ij}^* W_{ij} \\ \mathcal{L}_{ij}^* N_{ij} \end{bmatrix}. \quad (7)$$

Here, $W_{ij} \stackrel{\text{def}}{=} \lambda_{ij} - \tilde{\gamma}_{ij}$ and $N_{ij} \stackrel{\text{def}}{=} \zeta_{ij} - \tilde{\eta}_{ij}$ are differential tensors, with $\lambda_{ij} \stackrel{\text{def}}{=} 4\bar{\Delta}^2 (\tilde{S}_{ik} \tilde{\Omega}_{kj} + \tilde{S}_{jk} \tilde{\Omega}_{ki})$ and $\zeta_{ij} \stackrel{\text{def}}{=} 4\bar{\Delta}^2 (\tilde{S}_{ik} \tilde{S}_{kj} - \tilde{S}_{mn} \tilde{S}_{nm} \delta_{ij}/3)$. It has been demonstrated (Wang et al., 2005, 2006b) that DNM is capable of reflecting the correct level of turbulent kinetic energy (TKE) transfer (both forward and backward scattering) between the resolved and subgrid scales, and improving the numerical stability such that the DNM can be applied locally without resorting to the technique of plane averaging for calculating the model coefficients.

SGS Heat Flux Models

The focus of this research is on the SGS HF modelling rather than the SGS stress modelling. For this purpose, we propose two new models (i.e., a linear and a nonlinear dynamic SGS HF models). In order to perform a comparative study, the two proposed models are tested against the conventional DEDM-HF. All the SGS HF models investigated in this study can be categorized under the general framework of *tensor thermal diffusivity HF modelling* originally

introduced by Batchelor (1949), who suggested the following model for representing the turbulent HF vector $\langle u'_j \theta' \rangle_e$ in a Reynolds-averaged Navier-Stokes (RANS) approach:

$$\langle u'_j \theta' \rangle_e = -D_{jk} \frac{\partial \langle \theta \rangle_e}{\partial x_k}, \quad (8)$$

where D_{jk} is the so-called *turbulent tensor thermal diffusivity*, and $\langle \cdot \rangle_e$ represents an ensemble-averaged quantity in a RANS approach. An important application of Batchelor's suggestion is the GGDH model proposed by Daly and Harlow (1970), which models D_{jk} using the Reynolds stresses and expresses the turbulent heat flux vector as:

$$\langle u'_j \theta' \rangle_e = -C_\theta \mathcal{T}_e \langle u'_j u'_k \rangle_e \frac{\partial \langle \theta \rangle_e}{\partial x_k}, \quad (9)$$

where C_θ is a model coefficient, \mathcal{T}_e is an appropriate turbulent time scale, and $\langle u'_j u'_k \rangle_e$ is the Reynolds stress tensor.

SGS Heat Flux Model 1 (DEDM-HF):

The DEDM-HF proposed by Moin *et al.* (1991) expresses the SGS heat flux as

$$h_j = -C_\theta \bar{\Delta}^2 |\bar{S}| \frac{\partial \bar{\theta}}{\partial x_j}, \quad (10)$$

where the scalar eddy diffusivity implied by Eq. (10) is $\alpha_{sgs} = C_\theta \bar{\Delta}^2 |\bar{S}|$, which can be further written in a general tensor diffusivity form using the Kronecker delta as follows: $D_{jk} = \alpha_{sgs} \delta_{jk} = C_\theta \bar{\Delta}^2 |\bar{S}| \delta_{jk}$. Introducing the following base vector functions: $b_j \stackrel{\text{def}}{=} \bar{\Delta}^2 |\bar{S}| \frac{\partial \bar{\theta}}{\partial x_j}$ and $a_j \stackrel{\text{def}}{=} \tilde{\Delta}^2 |\tilde{S}| \frac{\partial \tilde{\theta}}{\partial x_j}$, the SGS HF vector at the grid-level can then be expressed as $h_j = -C_\theta b_j$. Similarly, the SGS HF vector at the test-grid-level ($H_j \stackrel{\text{def}}{=} \widetilde{\bar{u}_j \bar{\theta}} - \bar{u}_j \tilde{\theta}$) can be expressed as $H_j = -C_\theta a_j$. The grid- and test-grid-level SGS HF vectors satisfy the *vector identity*:

$$\mathcal{L}_j = H_j - \tilde{h}_j, \quad (11)$$

where $\mathcal{L}_j \stackrel{\text{def}}{=} \widetilde{\bar{u}_j \bar{\theta}} - \bar{u}_j \tilde{\theta}$ is directly computable in the simulation. By substituting the grid- and test-grid-level SGS HF models into the vector identity and assuming that $\tilde{h}_j = -\tilde{C}_\theta \tilde{b}_j \approx -C_\theta \tilde{b}_j$, a residual vector that expresses the difference between the left-hand-side (LHS) and right-hand-side (RHS) of Eq. (11) emerges: $\mathcal{E}_j = \mathcal{L}_j + C_\theta M_j$, where $M_j \stackrel{\text{def}}{=} a_j - \tilde{b}_j$ is a differential vector. By minimizing the norm of the residual vector (i.e., $\mathcal{E} \stackrel{\text{def}}{=} \mathcal{E}_j \mathcal{E}_j$) using the least squares method, the model coefficient can be obtained, viz.

$$C_\theta = -(\mathcal{L}_j M_j) / (M_j M_j). \quad (12)$$

SGS Heat Flux Model 2 (DGGDH-HF):

The original constitutive relation of Daly and Harlow (1970) is based on the Reynolds stress tensor for modelling the turbulent heat flux within the RANS approach. In the context of LES, this constitutive relation results in:

$$h_j = -C_\theta \mathcal{T} \tau_{jk}^* \frac{\partial \bar{\theta}}{\partial x_k}, \quad (13)$$

where \mathcal{T} is a characteristic subgrid time scale which is evaluated using the norm of the resolved velocity gradient tensor, viz. $\mathcal{T} = 1/|\bar{A}|$, with $\bar{A}_{ij} \stackrel{\text{def}}{=} \partial \bar{u}_i / \partial x_j$ and $|\bar{A}| \stackrel{\text{def}}{=} (2\bar{A}_{ij} \bar{A}_{ij})^{1/2}$. Equation (13) forms the constitutive relation for our proposed *dynamic GGDH model for representing the SGS heat flux* (DGGDH-HF). From Eq. (13), the tensor diffusivity for DGGDH-HF can be inferred as $D_{jk}^G = f(\tau_{jk}^*) = C_\theta \mathcal{T} \tau_{jk}^*$, which is a homogenous linear tensor function of τ_{jk}^* . Here, *homogeneity* refers to a linear transformation that obeys: $D_{jk}^G = f(\tau_{jk}^*) = \mathbf{0}$ if $\tau_{jk}^* = \mathbf{0}$. With the base vector functions defined as: $b_j^G \stackrel{\text{def}}{=} \frac{\tau_{jk}^*}{|\bar{A}|} \frac{\partial \bar{\theta}}{\partial x_k}$ and $a_j^G \stackrel{\text{def}}{=} \frac{\tau_{jk}^*}{|\tilde{A}|} \frac{\partial \tilde{\theta}}{\partial x_k}$, the grid- and test-grid-level SGS HF vectors can then be expressed succinctly as: $h_j = -C_\theta b_j^G$ and $H_j = -C_\theta a_j^G$, respectively.

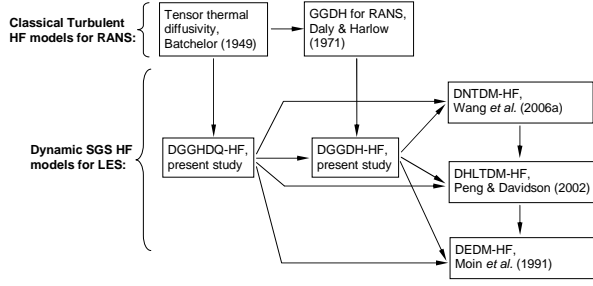


Fig. 1: Relationships between the classical turbulent HF models for RANS and dynamic SGS HF models for LES.

Here, $T_{jk}^* \stackrel{\text{def}}{=} (\widetilde{u_j u_k} - \tilde{u}_j \tilde{u}_k)^*$ represents the trace-free SGS stress tensor at the test-grid-level. Similarly, the optimal model coefficient C_θ can be obtained as

$$C_\theta = -(\mathcal{L}_j G_j)/(G_j G_j), \quad (14)$$

where $G_j \stackrel{\text{def}}{=} a_j^G - \tilde{b}_j^G$ is a differential vector.

SGS Heat Flux Model 3 (DGGDHQ-HF):

According to the theory of tensor functions, a vector-valued function of a second-order symmetric tensor \mathbf{M} and a vector \mathbf{v} can be represented by Noll's formula (Zheng, 1994) as follows:

$$\mathbf{h} = \varphi_0 \mathbf{v} + \varphi_1 \mathbf{M} \mathbf{v} + \varphi_2 \mathbf{M}^2 \mathbf{v}, \quad (15)$$

where φ_0 , φ_1 and φ_2 are functions of the independent irreducible tensor invariants of \mathbf{M} and \mathbf{v} . Noll's formula provides an explicit, inhomogeneous, complete and irreducible tensor function of \mathbf{M} and \mathbf{v} , forming the basis for our proposed *quadratic dynamic GGDH model for representing the SGS heat flux* (DGGDHQ-HF), viz.

$$h_j = -D_{jk}^Q \frac{\partial \bar{\theta}}{\partial x_k} - C_{\theta P} T |\tau| \frac{\partial \bar{\theta}}{\partial x_j} - C_{\theta G} T \tau_{jk}^* \frac{\partial \bar{\theta}}{\partial x_k} - C_{\theta Q} T \frac{\tau_{ji}^* \tau_{ik}^*}{|\tau|} \frac{\partial \bar{\theta}}{\partial x_k}, \quad (16)$$

where $|\tau| \stackrel{\text{def}}{=} (2\tau_{ij}^* \tau_{ij}^*)^{1/2}$ and the tensor diffusivity is a quadratic nonlinear tensor function of τ_{ij}^* , viz.

$$D_{jk}^Q = C_{\theta P} T |\tau| \delta_{jk} + C_{\theta G} T \tau_{jk}^* + C_{\theta Q} T \frac{\tau_{ji}^* \tau_{ik}^*}{|\tau|}. \quad (17)$$

The three terms on the RHS of Eq. (16) are identified as: the eddy diffusivity component (corresponding to the conventional DEDM-HF, or Model 1); the first-order tensor diffusivity component (corresponding to DGGDH-HF, or Model 2); and, the quadratic nonlinear component. Equations (15) and (17) are *inhomogeneous* owing to the presence of the SGS eddy diffusivity term (the term related to δ_{jk}), *irreducible* because none of \mathbf{v} , $\mathbf{M} \mathbf{v}$ and $\mathbf{M}^2 \mathbf{v}$ can be expressed as a single-valued function of the remaining terms, and *complete* because any vector function of the form $\mathbf{h} = f(\mathbf{M}, \mathbf{v})$ can be expressed by Eq. (15). As such, no higher-order terms (e.g., $\tau_{ji}^* \tau_{il}^* \tau_{lk}^* \cdot \partial \bar{\theta} / \partial x_k$) should appear in Eq. (17), since these are not independent of the existing terms.

Introducing the base vector functions: $b_j^P \stackrel{\text{def}}{=} \frac{|\tau|}{|A|} \frac{\partial \bar{\theta}}{\partial x_j}$, $a_j^P \stackrel{\text{def}}{=} \frac{|T|}{|A|} \frac{\partial \bar{\theta}}{\partial x_j}$, $b_j^Q \stackrel{\text{def}}{=} \frac{\tau_{ji}^* \tau_{ik}^*}{|\tau| |A|} \frac{\partial \bar{\theta}}{\partial x_k}$, $a_j^Q \stackrel{\text{def}}{=} \frac{T_{ji}^* T_{ik}^*}{|T| |A|} \frac{\partial \bar{\theta}}{\partial x_k}$, the grid- and test-grid level SGS heat fluxes can be simplified as

$$h_j = -C_{\theta P} b_j^P - C_{\theta G} b_j^G - C_{\theta Q} b_j^Q, \quad (18)$$

and

$$H_j = -C_{\theta P} a_j^P - C_{\theta G} a_j^G - C_{\theta Q} a_j^Q, \quad (19)$$

respectively. Here, $|T| = (2T_{ij}^* T_{ij}^*)^{1/2}$ is the norm of T_{ij}^* . By substituting Eqs. (18) and (19) into Eq. (11), a 3×3 matrix system for computing the model coefficients is directly obtained

$$[P_j, G_j, Q_j] \cdot [C_{\theta P}, C_{\theta G}, C_{\theta Q}]^T = -\mathcal{L}_j, \quad (20)$$

for $j = 1, 2$ and 3 . Here, $P_j \stackrel{\text{def}}{=} a_j^P - \tilde{b}_j^P$ and $Q_j \stackrel{\text{def}}{=} a_j^Q - \tilde{b}_j^Q$ are differential vectors. Because b_j^P , b_j^G and b_j^Q are linearly

Table 1: Summary of test cases for the validation of DGGDH-HF and DGGDHQ-HF ($Re_\tau = 150$)

Test case	SGS HF model	SGS stress model	Gr
Case 1	DEDM-HF	DM	1.3×10^6
Case 2	DGGDH-HF	DM	1.3×10^6
Case 3		DNM	1.3×10^6
Case 4		DNM	4.8×10^6
Case 5	DGGDHQ-HF	DM	1.3×10^6
Case 6		DNM	1.3×10^6
Case 7		DNM	4.8×10^6

independent as are a_j^P , a_j^G and a_j^Q , the differential vectors P_j , G_j and Q_j are also linearly independent. Therefore, the solution of Eq. (20) for the three model coefficients exists locally for an instantaneous turbulent thermal flow.

Relations between Different SGS HF Models

Figure 1 illustrates the relation between the RANS and LES HF models discussed in this research. As shown in this figure, all these models are unified under the general framework of tensor thermal diffusivity HF modelling proposed by Batchelor [cf. Eq. (8)]. A direct implementation of Daly and Harlow's approach in the context of LES results in the proposed DGGDH-HF, which by analogy assumes D_{ij} to be proportional to τ_{ij} (or, its trace-free form τ_{ij}^*). An extension of the GGDH constitutive relation from a linear to a quadratic form results in the proposed DGGDHQ-HF, which corresponds to the most general modelling equation for any explicit algebraic constitutive relation that is based on only τ_{ij} and $\partial \bar{\theta} / \partial x_j$ [viz., $h_j = f(\tau_{ij}, \partial \bar{\theta} / \partial x_j)$].

On adoption of the classical Smagorinsky constitutive relation, the SGS stress tensor assumes the classical form $\tau_{ij}^* = -2C_S \bar{\Delta}^2 |\bar{S}| \bar{S}_{ij}$. Substituting this model into DGGDHQ-HF and evaluating the SGS time scale as $T = 1/|\bar{S}|$ results in an equivalent form for DNTDM-HF of Wang *et al.* (2006a):

$$h_j = -D_{jk}^N \frac{\partial \bar{\theta}}{\partial x_k} - C'_{\theta P} \bar{\Delta}^2 |\bar{S}| \frac{\partial \bar{\theta}}{\partial x_j} - C'_{\theta G} \bar{\Delta}^2 \bar{S}_{jk} \frac{\partial \bar{\theta}}{\partial x_k} - C'_{\theta Q} \bar{\Delta}^2 \frac{\bar{S}_{ji} \bar{S}_{ik}}{|\bar{S}|} \frac{\partial \bar{\theta}}{\partial x_k}. \quad (21)$$

The derivation of DEDM-HF of Moin *et al.* (1991) and DHLTDM-HF of Peng and Davidson (2002) as special cases of our general modelling approach (i.e., DGGDHQ-HF, DGGDH-HF and DNTDM-HF) is straightforward. For example, if $C'_{\theta G} = C'_{\theta Q} = 0$, DNTDM-HF reduces to DEDM-HF; and, if $C'_{\theta P} = C'_{\theta Q} = 0$, DNTDM-HF reduces to DHLTDM-HF with

$$h_j = -D_{jk}^{HL} \frac{\partial \bar{\theta}}{\partial x_k} = -C'_{\theta G} \bar{\Delta}^2 \bar{S}_{jk} \frac{\partial \bar{\theta}}{\partial x_k}, \quad (22)$$

where the tensor diffusivity is a homogeneous linear tensor function of \bar{S}_{ij} , viz. $D_{jk}^{HL} = f(\bar{S}_{jk}) = C'_{\theta G} \bar{\Delta}^2 \bar{S}_{jk}$.

TEST CASE AND NUMERICAL ALGORITHM

In order to validate the proposed SGS HF models, numerical simulations have been performed using a benchmark test case of a fully developed unstably stratified turbulent channel flow. The results are compared with the DNS data of Iida and Kasagi (1997, designated as IK-1997). The dimensions of the computational domain are $L_1 \times L_2 \times L_3 = 5\pi\delta \times 2\delta \times 2\pi\delta$ in the streamwise (x_1), wall-normal (x_2) and spanwise (x_3) directions, respectively. Here, the half channel width δ is 40 mm. A coarse grid of $48 \times 32 \times 48$ nodes has been used for discretization of the computational domain. The grid system is uniform in the streamwise and spanwise directions, and is refined in the wall-normal direction within the near-wall region. The flow is characterized by a Reynolds number of $Re_\tau = 150$. To examine the effects of buoyancy on the heat and fluid flow, two Grashof numbers (i.e., $Gr = 1.3 \times 10^6$ and 4.8×10^6) are tested. The

Reynolds and Grashof numbers are defined as $Re_\tau = u_\tau \delta / \nu$ and $Gr = g\beta\Delta\theta(2\delta)^3/\nu^2$, respectively. Here, u_τ represents the wall friction velocity, and $\Delta\theta = \theta_{wh} - \theta_{wc}$ is the temperature difference between the hot and cold walls.

The governing equations were discretized using a second-order finite volume method. The filtered momentum equations were solved using a fractional-step method, whereby the nonlinear advection term was discretized using a second-order explicit Adams-Bashforth scheme and the viscous diffusion term was discretized using a second-order Crank-Nicolson scheme. The pressure correction equation was solved using a multigrid method, and checkerboard oscillations in the pressure field arising from a state of pressure-velocity decoupling on a collocated grid were removed using a momentum interpolation scheme. To solve the filtered thermal energy equation, a fourth-order Runge-Kutta method was used to advance the temperature field over a single time step. The time period used to obtain the turbulent flow and temperature statistics was based on 30,000 time steps. In presentation of the results, quantities non-dimensionalized using the friction velocity u_τ and friction temperature $T_\tau \stackrel{\text{def}}{=} q_w/(\rho c_P u_\tau)$ are denoted with a superscript “+”. Here, q_w is the wall heat flux and c_P is the specific heat at constant pressure. Table 1 summarizes the seven test cases considered in this research.

RESULT ANALYSIS

Resolved Velocity and Temperature Fields

Figure 2 shows the time-averaged velocity field and isopleths of the resolved temperature field in the x_2 - x_3 plane at the center of the channel. From Fig. 2, we observe two symmetrical large longitudinal vortex rolls aligned along the streamwise direction, which result in a downdraft in the central region and two updrafts in the peripheral regions. These two large longitudinal vortex rolls are a consequence of the joint effects of buoyancy and the streamwise pressure gradient, and give rise to the pattern of large organized secondary structures that are characteristic of this flow.

Figure 3 shows the mean resolved streamwise velocity profiles (i.e., $\langle \bar{u}_1 \rangle$) predicted using the two proposed SGS HF models. As shown in Fig. 3, owing to the existence of buoyancy, the predicted velocity profiles deviate from the familiar log law. Although the velocity profiles predicted by the different models agree in general, slight differences exist. The predictions of $\langle \bar{u}_1 \rangle$ obtained using the combinations of DGGDH-HF with DNM (case 3) and DGGDHQ-HF with DNM (case 6) are in better conformance with the DNS data than predictions obtained using the other SGS stress and HF model combinations. Comparatively speaking, the conventional (and popular) SGS model combination of DEDM-HF with DM (case 1) gives the worst prediction of the velocity profile. A perusal and comparison of the five different SGS model combinations tested suggests that use of an advanced SGS stress model and/or an advanced SGS HF model improves the predictions of the resolved mean velocity field. More specifically, (i) by comparing case 2 with case 3, and case 5 with case 6, we observe that it is advantageous to use DNM for modelling the SGS stress tensor as it leads to a better predictive performance; (ii) by comparing cases 2 and 5 with case 1, we observe that it is advantageous to use the proposed DGGDH-HF or DGGDHQ-HF for modeling the SGS heat flux as both these models lead to improved predictions; and, (iii) as mentioned above, use of the combination of DGGDH-HF with DNM (case 3) or of DGGDHQ-HF with DNM (case 6) gives results that are in the best conformance with the DNS data.

Figure 4 demonstrates the effects of buoyancy on the mean resolved velocity profile predicted using the two best

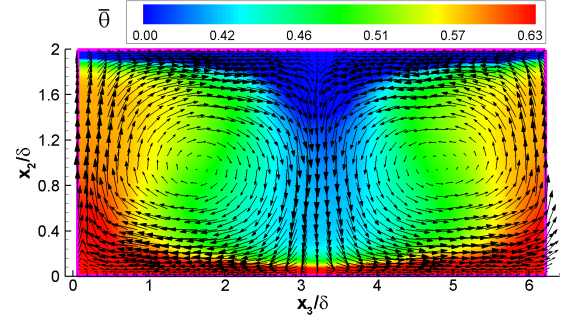


Fig. 2: Velocity field and isopleths of the resolved temperature field (x_2 - x_3 view at $x_1/L_1 = 0.49$, predicted using DGGDH-HF & DNM, $Gr = 1.3 \times 10^6$, temperature is normalized using the temperature difference between the two walls).

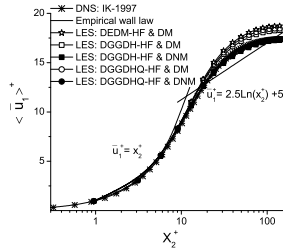


Fig. 3: Mean profiles of the resolved streamwise velocity ($Gr = 1.3 \times 10^6$).

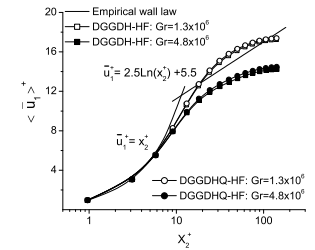
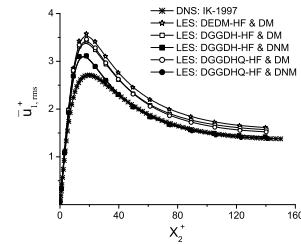
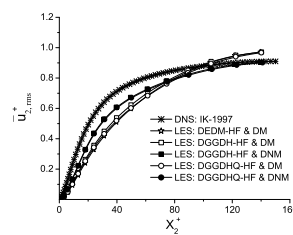


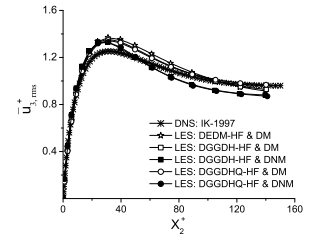
Fig. 4: Effect of Grashof number on the mean resolved velocity (SGS stress model: DNM).



(a) Streamwise component



(b) Wall-normal component



(c) Spanwise component

Fig. 5: Resolved turbulence intensities ($Gr = 1.3 \times 10^6$).

performance combinations of the SGS stress and HF models observed in Fig. 3 (namely, the combinations of DGGDH-HF with DNM and of DGGDHQ-HF with DNM). From Fig. 4, it is seen that the performance of the DGGDH-HF and DGGDHQ-HF is similar at the two different Grashof numbers. As Grashof number increases, the non-dimensionalized streamwise velocity shifts downwards in response to the increase in the buoyancy. Figure 5 compares the predicted resolved turbulence intensities [or, root-mean-square (RMS) values, which are defined as $\bar{u}_{i,rms}^+ \stackrel{\text{def}}{=} \langle (\bar{u}_i - \langle \bar{u}_i \rangle)^2 \rangle^{1/2}$ for $i = 1, 2$ and 3] with the DNS data. In agreement with our previous conclusion based on the mean resolved streamwise velocity profiles, it appears that under exactly the same test condition, the predictions of $\bar{u}_{i,rms}$ using the combinations of DGGDH-HF with DNM (case 3) and DGGDHQ-HF with DNM (case 6) are in better conformance with the DNS data than those obtained using the other model combinations.

Figure 6 shows the profile of the mean resolved temperature across the channel. Due to the effect of buoyancy, the mean temperature profile deviates from the conventional law of the wall relationship. Among the five modelling combinations tested, predictions obtained using the three combinations based on DM (cases 1, 2 and 5) slightly over-predict the temperature in comparison with the DNS data. Although the combinations of DGGDH-HF with DNM (case 3) and DGGDHQ-HF with DNM (case 6) slightly under-predict the resolved temperature, these two combinations nevertheless provide slightly better predictions of the resolved temperature profile in comparison with the DNS data, especially in the buffer layer ($x_2^+ \approx 10$ –30). Figure 7 displays the resolved temperature fluctuation (RMS of $\bar{\theta}$): $\bar{\theta}_{rms}^+ \stackrel{\text{def}}{=} ((\frac{\bar{\theta} - \langle \bar{\theta} \rangle}{T_r})^2)^{1/2}$. In conformance with previous observations, cases 3 and 6 generally provide better predictions than the other three tested cases (which all use DM), when compared with the DNS data. In particular, predictions obtained using the combination of DGGDHQ-HF with DNM (case 6) are in the best agreement with the DNS data, especially in the buffer layer. This implies that for LES of heat transfer (or, scalar transport), it is beneficial to use an advanced SGS stress model (such as DNM) in the filtered momentum equation to obtain a more realistic fluid flow field.

Budgets of Shear Stresses and Heat Fluxes

For LES of a channel flow, an instantaneous filtered quantity can be decomposed into a time- and plane-averaged component and a residual component as: $\bar{\phi} = \langle \bar{\phi} \rangle + \bar{\phi}''$. On assuming that the flow is statistically stationary and homogeneous in the x_1 – x_3 plane, an equation which balances the time- and plane-averaged shear stresses at an arbitrary wall-normal location x_2 can be obtained from the filtered streamwise momentum equation:

$$\nu \frac{\partial \langle \bar{u}_1 \rangle}{\partial x_2} - \langle \bar{u}_1'' \bar{u}_2'' \rangle - \langle \tau_{12} \rangle = \frac{1}{\rho} \frac{\partial \langle \bar{p} \rangle}{\partial x_1} x_2 + \frac{\tau_{wh}}{\rho}. \quad (23)$$

The three terms on the LHS of Eq. (23) represent the resolved viscous shear stress, resolved Reynolds (or, turbulent) shear stress, and SGS shear stress, respectively. The two terms on the RHS of the equation represent the resolved integrated force due to the mean pressure gradient, and the resolved viscous shear stress at the hot wall ($\tau_{wh} = \rho \nu \frac{\partial \langle \bar{u}_1 \rangle}{\partial x_2} |_{x_2=0}$), respectively.

Figures 8(a) and (b) show the shear stress budget predicted using DGGDH-HF and DGGDHQ-HF, respectively. All the terms shown in the figures are non-dimensionalized using the viscous shear stress term [i.e., $\tau_w/\rho = u_\tau^2$]. Although two assumptions were used in the derivation of Eq. (23) from the filtered momentum equation, the balance expressed by this equation is consistent with the results obtained from the numerical simulation. As evident in both Figs. 8(a) and (b), the total shear stress calculated from the LHS of Eq. (23) agrees very well with that calculated from the RHS of the equation. The time- and plane-averaged SGS shear stress component $\langle -\tau_{12} \rangle$ is very small in comparison with the other shear stress components. However, as shown in Figs. 8(a) and (b), the instantaneous value of the SGS shear stress $-\tau_{12}$ can be significant at a specific location (illustrated using a dashed line).

The time- and plane-averaged equation expressing the balance in the mean wall-normal heat fluxes at any arbitrary wall-normal location x_2 can be obtained from the filtered thermal energy equation [i.e., Eq. (3)] as:

$$-\alpha \frac{\partial \langle \bar{\theta} \rangle}{\partial x_2} + \langle \bar{u}_2'' \bar{\theta}'' \rangle + \langle h_2 \rangle = \frac{q_{wh}}{\rho c_P}, \quad (24)$$

where $q_{wh} \stackrel{\text{def}}{=} -\lambda \frac{\partial \langle \bar{\theta} \rangle}{\partial x_2} |_{x_2=0}$ is the resolved molecular heat flux at the hot wall, and λ is the thermal conductivity. The

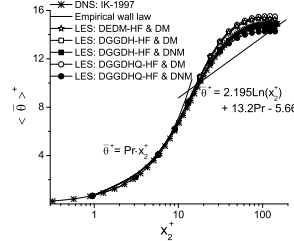


Fig. 6: Mean profiles of the resolved temperature ($Gr = 1.3 \times 10^6$).

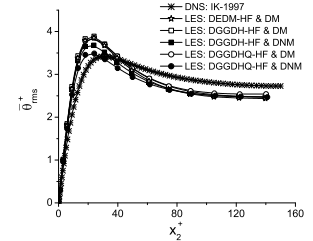
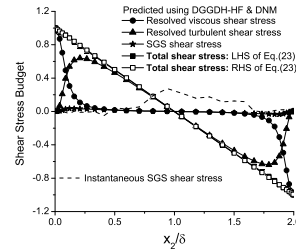
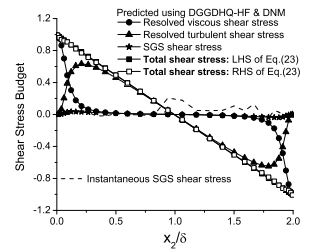


Fig. 7: Root-mean-square of the resolved temperature ($Gr = 1.3 \times 10^6$).

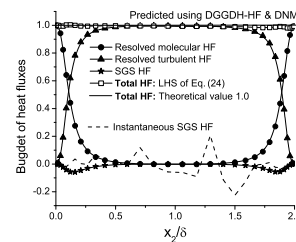


(a) DGGDH-HF

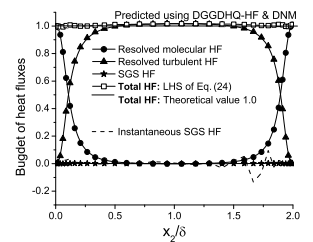


(b) DGGDHQ-HF

Fig. 8: Budget of wall-normal shear stresses (SGS stress model: DNM, $Gr = 1.3 \times 10^6$, location for the instantaneous SGS shear stress distribution is: $x_1/L_1 = x_3/L_3 = 0.49$).



(a) DGGDH-HF



(b) DGGDHQ-HF

Fig. 9: Budget of wall-normal heat fluxes (SGS stress model: DNM, $Gr = 1.3 \times 10^6$, location for the instantaneous SGS shear stress distribution is: $x_1/L_1 = x_3/L_3 = 0.49$).

three wall-normal HF components on the LHS of Eq. (24) correspond to the resolved molecular heat flux, resolved turbulent heat flux, and SGS heat flux, respectively. Figure 9 displays the budget of the wall-normal heat flux terms predicted by DGGDH-HF and DGGDHQ-HF. All the terms shown in the figure are non-dimensionalized by the molecular heat flux at the hot wall, i.e. $q_{wh}/\rho c_p = u_{\tau h} T_{\tau h}$. With this normalization, the total heat flux given by the RHS of Eq. (24) becomes unity. As shown in Figs. 9(a) and (b), both DGGDH-HF and DGGDHQ-HF provide a good balance of the wall-normal heat fluxes, since it is evident from these figures that the total heat flux calculated from the LHS of Eq. (24) agrees well with the theoretical value of 1.0. Figures 9(a) and (b) also show that the instantaneous values of the wall-normal SGS HF h_2 can fluctuate locally with a relatively large amplitude in sharp contrast to the time- and plane-averaged values $\langle h_2 \rangle$.

Figures 10(a) and (b) show the streamwise and wall-normal turbulent heat fluxes (i.e., $\langle \bar{u}_1'' \bar{\theta}'' \rangle^+ + \langle h_1 \rangle^+$ and $\langle \bar{u}_2'' \bar{\theta}'' \rangle^+ + \langle h_2 \rangle^+$, respectively) using wall coordinates in comparison with the DNS results. Although the performance of the five different SGS model combinations is very similar in terms of their predictions of the wall-normal HF component [cf. Fig. 10(b)] (all in good agreement with the DNS results), distinct differences exist between their predictions of the streamwise component of turbulent HF [cf. Fig. 10(a)]. Once again, it is observed that use of DNM and/or use of the proposed DGGDH-HF and DGGDHQ-HF

gives predictions of the streamwise turbulent heat flux that are in better agreement with the DNS data.

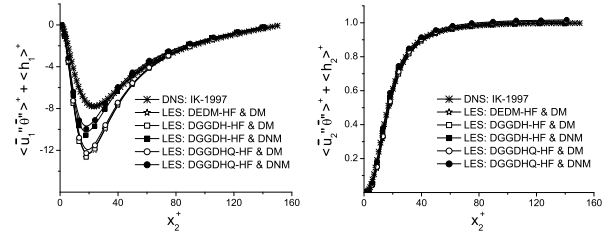
SGS Effect on Local TKE Flux

The rate of local TKE flux between the resolved and unresolved scales is represented by an invariant of τ_{ij}^* and \bar{S}_{ij} through tensor contraction, viz. $P_r \stackrel{\text{def}}{=} -\tau_{ij}^* \bar{S}_{ij}$. This quantity represents an inertial inviscid local energy flux between the resolved scale and unresolved subgrid scales. Figures 11(a) and (b) shows the time- and plane-averaged value of P_r across the channel (non-dimensionalized using u_τ^4/ν). The forward scatter (i.e., $\langle P_r^+ \rangle$) and backscatter (i.e., $\langle P_r^- \rangle$) of TKE have been separated, and naturally, these two quantities must verify $\langle P_r \rangle = \langle P_r^+ \rangle + \langle P_r^- \rangle$. From the Fig. 11, it is observed that both SGS model combinations of DGGDH-HF with DNM (case 3) and DGGDHQ-HF with DNM (case 6) are capable of reflecting backscatter. In contrast, due to the simplicity and limitation of the constitutive relation inherent to DM (which requires the principal axes of $-\tau_{ij}^*$ be aligned with those of \bar{S}_{ij}), none of the combinations of the SGS models based on DM (not shown in the figures) can successfully predict the net effect of backscatter in a time- and plane-averaged sense. By comparing Figs. 11(a) and (b), it is observed that the magnitude of local TKE fluxes predicted by DGGDH-HF and DNM are slightly larger than those predicted by DGGDHQ-HF and DNM, reflecting differences in the SGS HF modelling effect on local TKE transport.

CONCLUSIONS

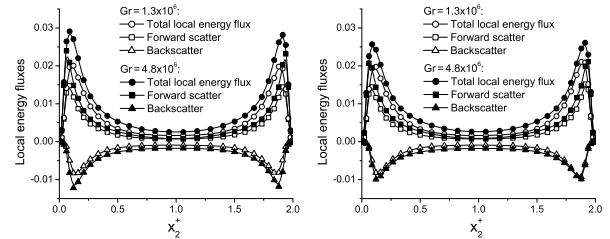
The proposed DGGDHQ-HF derived from Noll's formula provides the most general representation of the SGS heat flux for the family of explicit algebraic models that are functions of the resolved temperature gradient $\partial\bar{\theta}/\partial x_j$ and SGS stress tensor τ_{ij} [viz., $h_j = f(\tau_{ij}, \partial\bar{\theta}/\partial x_j)$]. The representation of the SGS heat flux by DGGDHQ-HF is explicit, nonlinear (quadratic), inhomogeneous, complete and irreducible. One of the important special cases of DGGDHQ-HF is DGGDH-HF, which is a linear homogeneous tensor diffusivity model that is analogous to the well-known GGDH approach of Daly and Harlow (1970) as applied within the RANS framework. We demonstrate that the proposed DGGDH-HF and DGGDHQ-HF are general linear and nonlinear SGS HF modelling approaches, which include as special cases a number of previous models such as DEDM-HF of Moin *et al.* (1991), DHLTDM-HF of Peng and Davidson (2002) and DNTDM-HF of Wang *et al.* (2006a).

In order to validate the proposed modelling approach, a comparative numerical study has been conducted based on an unstably stratified horizontal channel flow. It is observed that the performance of DGGDHQ-HF and DGGDH-HF is superior to that provided by the conventional DEDM-HF. Also, in comparison with the conventional DM of Lilly (1992), use of DNM can improve predictions of both the velocity and temperature fields. On utilization of DNM for modelling the SGS stress, the predictive performance of DGGDHQ-HF and DGGDH-HF is generally comparable for the flow simulated in this study, although it should be noted that the performance of DGGDHQ-HF is slightly better than that of DGGDH-HF in terms of the prediction of RMS of the resolved temperature field ($\bar{\theta}_{rms}^+$) and the streamwise turbulent heat flux ($\langle \bar{u}_1' \bar{\theta}' \rangle^+ + \langle h_1 \rangle^+$). With respect to the need for advancing the theory of constitutive relations for SGS HF modelling, both DGGDH-HF and DGGDHQ-HF represent important generalizations to the current state-of-the-art for SGS HF modelling. However, if attention is solely focused on computational cost, DGGDH-HF appears to be more appealing since this model requires fewer numerical operations for its implementation than does DGGDHQ-HF.



(a) Streamwise component (b) Wall-normal component

Fig. 10: Turbulent heat fluxes ($Gr = 1.3 \times 10^6$).



(a) DGGDH-HF

(b) DGGDHQ-HF

Fig. 11: Local TKE fluxes predicted by the proposed SGS HF models (SGS stress model: DNM; $Gr = 1.3 \times 10^6$). Total: $\langle P_r \rangle / (u_\tau^4 / \nu)$; forward scatter: $\langle P_r^+ \rangle / (u_\tau^4 / \nu)$; backscatter: $\langle P_r^- \rangle / (u_\tau^4 / \nu)$.

REFERENCES

- Batchelor, G. K., 1949, "Diffusion in a field of homogeneous turbulence", *Austral. J. Sci. Res. A*, vol. 2, pp. 437–450.
- Daly, B. J. and Harlow, F. H., 1970, "Transport equations in turbulence", *Phys. Fluids*, vol. 13, pp. 2634–2649.
- Germano, M., Piomelli, U., Moin, P. and Cabot, W. H., 1991, "A dynamic subgrid-scale eddy viscosity model", *Phys. Fluids A*, vol. 3, pp. 1760–1765.
- Iida, O. and Kasagi, N., 1997, "Direct numerical simulation of unstably stratified turbulent channel flow", *ASME J. Heat Trans.*, vol. 119, pp. 53–61, DNS data available from www.thtlab.t.u-tokyo.ac.jp.
- Kang, H. S. and Meneveau, C., 2002, "Universality of large eddy simulation model parameters across a turbulent wake behind a heated cylinder", *J. Turbul.*, vol. 3 (32), pp. 1–27.
- Lilly, D. K., 1992, "A proposed modification of the Germano subgrid-scale closure method", *Phys. Fluids A*, vol. 4, pp. 633–635.
- Moin, P., Squires, K., Cabot, W. and Lee, S., 1991, "A dynamic subgrid-scale model for compressible turbulence and scalar transport", *Phys. Fluids A*, vol. 3, pp. 2746–2757.
- Peng, S.-H. and Davidson, L., 2002, "On a subgrid-scale heat flux model for large eddy simulation of turbulent thermal flow", *Int. J. Heat Mass Trans.*, vol. 45, pp. 1393–1405.
- Porté-Agel, F., Parlange, M. B., Meneveau, C. and Eichinger, W. E., 2001, "A priori field study of the subgrid-scale heat fluxes and dissipation in the atmospheric surface layer", *J. Atmos. Sci.*, vol. 58, pp. 2673–2698.
- Salveti, M. V. and Banerjee, S., 1995, "A priori tests of a new dynamic subgrid-scale model for finite-difference large-eddy simulation", *Phys. Fluids*, vol. 7, pp. 2831–2847.
- Wang, B.-C. and Bergstrom, D. J., 2005, "A dynamic nonlinear subgrid-scale stress model", *Phys. Fluids*, vol. 17(035109), pp. 1–15.
- Wang, B.-C., Yin, J., Yee, E. and Bergstrom, D. J., 2006a, "A new irreducible dynamic nonlinear tensor-diffusivity SGS heat-flux model for LES of convective flows", in *Proc. 5th Int. Symp. Turbul., Heat Mass Trans.*, K. Hanjalić *et al.*, ed., Dubrovnik, Croatia, 14 pages.
- Wang, B.-C., Bergstrom, D. J., Yin, J. and Yee, E., 2006b, "Turbulence topologies predicted using large eddy simulations", *J. Turbul.*, vol. 7(34), pp. 1–28.
- Wang, B.-C., Yee, E., Yin, J. and Bergstrom, D. J., 2007, "A general dynamic linear tensor-diffusivity subgrid-scale heat-flux model for large-eddy simulation of turbulent thermal flows", *Numer. Heat Trans.: Part B*, vol. 51, pp. 205–227.
- Zheng, Q.-S., 1994, "Theory of representations for tensor functions—a unified invariant approach to constitutive equations", *Appl. Mech. Rev.*, vol. 47, pp. 545–587.